

Direct inhibition of myosin II effectively blocks glioma invasion in the presence of multiple motogens

Sanja Ivkovic^a, Christopher Beadle^a, Sonal Noticewala^b, Susan C. Massey^c, Kristin R. Swanson^{c,d}, Laura N. Toro^e, Anne R. Bresnick^e, Peter Canoll^b, and Steven S. Rosenfeld^{a,b}

^aDepartment of Neurology and ^bDepartment of Pathology and Cell Biology, Columbia University, New York, NY 10032; ^cDepartment of Applied Mathematics and ^dDepartment of Pathology, University of Washington, Seattle, WA 98195; ^eDepartment of Biochemistry, Albert Einstein College of Medicine, Bronx, NY 10461

ABSTRACT Anaplastic gliomas, the most common and malignant of primary brain tumors, frequently contain activating mutations and amplifications in promigratory signal transduction pathways. However, targeting these pathways with individual signal transduction inhibitors does not appreciably reduce tumor invasion, because these pathways are redundant; blockade of any one pathway can be overcome by stimulation of another. This implies that a more effective approach would be to target a component at which these pathways converge. In this study, we have investigated whether the molecular motor myosin II represents such a target by examining glioma invasion in a series of increasingly complex models that are sensitive to platelet-derived growth factor, epidermal growth factor, or both. Our results lead to two conclusions. First, malignant glioma cells are stimulated to invade brain through the activation of multiple signaling cascades not accounted for in simple *in vitro* assays. Second, even though there is a high degree of redundancy in promigratory signaling cascades in gliomas, blocking tumor invasion by directly targeting myosin II remains effective. Our results thus support our hypothesis that myosin II represents a point of convergence for signal transduction pathways that drive glioma invasion and that its inhibition cannot be overcome by other motility mechanisms.

Monitoring Editor

Yu-Li Wang
Carnegie Mellon University

Received: Jan 14, 2011

Revised: Dec 14, 2011

Accepted: Dec 21, 2011

INTRODUCTION

Glioblastoma multiforme (GBM) is the most common and malignant of glial tumors, and it continues to be associated with a dismal prognosis (Buckner *et al.*, 2007; Stupp *et al.*, 2007). Although genetic heterogeneity of tumor cells, insensitivity to alkylating chemotherapeutics, and the blood–brain barrier all contribute to this

situation, an additional factor is the propensity of GBMs to disperse widely within the brain (Scherer, 1940; Burger and Kleihues, 1989; Hoelzinger *et al.*, 2007). Tumor invasion limits the efficacy of local therapies, such as surgery and radiosurgery (Burger *et al.*, 1983; Giese and Westphal, 1996), and it can be additionally accelerated with antiangiogenic therapies, which have entered widespread clinical use (Norden *et al.*, 2008; Reardon *et al.*, 2008). Thus, preventing GBM dispersion has the potential for converting this tumor from an invasive, uncontrollable disease to a local disease that might be more effectively treated with currently available, local therapies, including surgery and radiation (Lim *et al.*, 2007).

Among the most common genetic alterations found in GBMs are amplification and/or constitutive activation of signal transduction pathways activated by epidermal growth factor (EGF), platelet-derived growth factor (PDGF), and hepatocyte growth factor (HGF; Cancer Genome Atlas Research Network, 2010). Each of these ligands can stimulate glioma cell motility and invasion (Hoelzinger *et al.*, 2007). Furthermore, recent studies have demonstrated that in

This article was published online ahead of print in MBcC in Press (<http://www.molbiolcell.org/cgi/doi/10.1091/mbc.E11-01-0039>) on January 4, 2012.

Address correspondence to: Steven S. Rosenfeld (rosenfsc@ccf.org).

Abbreviations used: DAPI, 4,6-diamidino-2-phenylindole; dpi, days postinjection; EGF, epidermal growth factor; EGFR, epidermal growth factor receptor; GAPDH, glyceraldehyde-3-phosphate dehydrogenase; GBM, glioblastoma multiforme; GFP, green fluorescent protein; HGF, hepatocyte growth factor; LPA, lysophosphatidic acid; MSD, mean square displacement; PBS, phosphate-buffered saline; PDGF, platelet-derived growth factor; PDGFR, platelet-derived growth factor receptor; ROCK, Rho kinase; RTK, receptor tyrosine kinase.

© 2012 Ivkovic *et al.* This article is distributed by The American Society for Cell Biology under license from the author(s). Two months after publication it is available to the public under an Attribution–Noncommercial–Share Alike 3.0 Unported Creative Commons License (<http://creativecommons.org/licenses/by-nc-sa/3.0>).

“ASCB®,” “The American Society for Cell Biology®,” and “Molecular Biology of the Cell®” are registered trademarks of The American Society of Cell Biology.

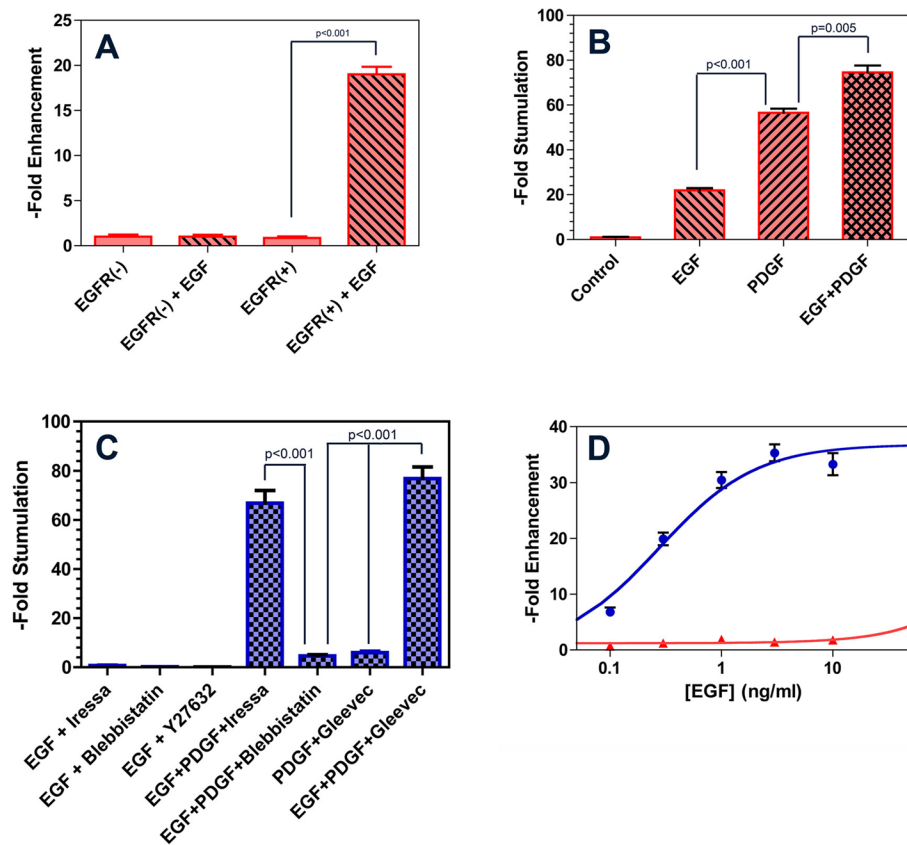


FIGURE 1: Effect of growth factor receptor stimulation and its inhibition on Transwell migration of C6 glioma cells. (A) C6 glioma cells expressing EGFR-mCherry (EGFR(+)) and untransfected C6 cells (EGFR(-)) were seeded into the upper part of a 3- μ m-pore Transwell chamber. Migration across the Transwell membrane was measured after a 5-h incubation by staining the cells with 4,6-diamidino-2-phenylindole and counting the number of nuclei in 10 high-power fields. Data were normalized to the mean of EGFR(-) cells in the absence of EGF and expressed as fold enhancement. Bars represent mean \pm 1 SD. EGFR(+) cells showed increased migration in response to EGF (10 ng/ml) compared with no EGF ($p < 0.001$). In comparison, EGFR(-) cells showed no appreciable migratory response to EGF ($p = 1.00$). (B) Transwell migration of EGFR(+) cells was monitored in the absence of serum or growth factor stimulation (Control), in the presence of 10 ng/ml EGF or 100 ng/ml PDGF, and in the presence of both (PDGF+EGF). Data were normalized to the mean of the control condition and expressed as fold enhancement. Bars represent mean \pm 1 SD. Differences between EGF and PDGF conditions ($p < 0.001$) and between PDGF and EGF plus PDGF conditions ($p < 0.005$) were statistically significant. (C) Transwell migration in the presence of EGF, PDGF, and its cognate receptor inhibitors. While the EGFR tyrosine kinase inhibitor Iressa (10 μ M) blocks Transwell migration in the presence of EGF, its effects are negated by addition of PDGF. Likewise, the PDGFR inhibitor Gleevec (20 μ M) blocks PDGF-stimulated Transwell migration. Blebbistatin (10 μ M) and Y27632 (50 μ M) are also effective in the presence of EGF stimulation. Furthermore, unlike Iressa and Gleevec, blebbistatin also remains effective in the presence of combined EGF and PDGF stimulation. (D) Dose-response relationship for EGF-stimulated Transwell migration of EGFR(+) cells. Migration in response to EGF can be fit to a hyperbolic isotherm, defining an EC_{50} of 0.28 ± 0.04 ng/ml (blue curve). In the presence of 10 μ M blebbistatin (red curve), migration remains inhibited by $> 90\%$ over a range of EGF that spans two orders of magnitude.

many GBMs, multiple receptor tyrosine kinases (RTKs) are coactivated (Stommel et al., 2007), producing a degree of signal transduction redundancy. Furthermore, GBMs are generally heterogeneous tumors, and only a fraction of tumor cells within any given tumor express amplified or constitutively activated RTKs. It seems likely that this redundancy and heterogeneity contribute to the finding that clinical trials utilizing single RTK inhibitors have produced responses that are neither universal nor durable (de Groot and Gilbert, 2007; Reardon et al., 2008).

EGF (10 ng/ml), PDGF (100 ng/ml), and the combination of both in what appears to be an additive manner. (Figure 1B). As Figure 1C illustrates, addition of the EGFR tyrosine kinase inhibitor Iressa (10 μ M) inhibits EGF-stimulated migration in this assay, as do the direct myosin II inhibitor blebbistatin and an inhibitor of Rho kinase (ROCK; Y27632), which is an immediate upstream activator of myosin II. However, PDGF restores Transwell migration to levels similar to those seen in the presence of PDGF alone. Likewise, while the PDGFR inhibitor Gleevec neutralizes the promigratory effects of

In our previous study (Beadle et al., 2008), we demonstrated that the molecular motor myosin II contributes to the process of glioma invasion by generating the internal compressive forces needed to extrude the cell body and nucleus through the small intercellular spaces that characterize brain parenchyma. Myosin II is a point at which many promigratory signal transduction pathways that are dysregulated in GBM converge, and it is widely expressed in malignant gliomas (Beadle et al., 2008). As a point of convergence, it should not be redundant, and its direct inhibition should block GBM invasion regardless of how many upstream promigratory signal transduction cascades are active. However, cycles of actin polymerization can also drive cell motility (Svitkina et al., 1997). Furthermore, we have shown that myosin II activity is not required when glioma cells migrate in a barrier-free environment, such as on the surface of a coverslip (Beadle et al., 2008). Thus it remains unclear whether sufficient upstream activation of signal transduction pathways might be able to overcome a need for myosin II in glioma invasion by activating other motility mechanisms that do not utilize this molecular motor.

In this study, we have addressed this issue by examining how progressively increasing signal transduction activity affects glioma cell invasion and the need for myosin II in this process, both in vitro and in situ within brain parenchyma. Our results support our hypothesis that myosin II is an indispensable component of the glioma invasion apparatus, and remains so in spite of activation of multiple upstream, promigratory pathways relevant to the biology of human GBM.

RESULTS

C6 glioma invasion using in vitro Transwell assays

We generated a C6 glioma cell line that was stably transfected with a vector encoding for epidermal growth factor receptor-green fluorescent protein (EGFR-GFP). Transfection of these cells induced an EGF-responsive migration across 3- μ m Transwell membranes (Figure 1A). These cells also express platelet-derived growth factor receptor α (PDGFR α ; Strawn et al., 1994), and their migration in this assay responds to

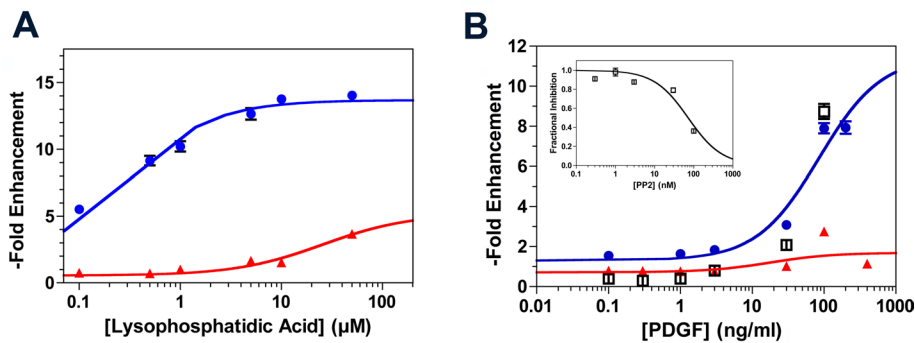


FIGURE 2: Dose–response of LPA and PDGF-stimulated Transwell migration of EGFR(+) C6 glioma cells in the absence and presence of myosin II inhibition. (A) Migration of C6 cells through 3-µm Transwell pores after 5 h of incubation demonstrates a hyperbolic dose–response relationship to LPA concentration (blue), defining an EC_{50} of 0.20 ± 0.02 µM. In the presence of 10 µM blebbistatin (red), this migration is reduced by >75%, even at saturating doses of LPA. Data were normalized to the mean of cells migrating in the absence of LPA and expressed as fold enhancement. (B) Corresponding experiment with PDGF also demonstrates a hyperbolic dose–response relationship (blue), defining an EC_{50} of 126 ± 47 ng/ml. As with LPA, 10 µM blebbistatin (red) reduces Transwell migration by > 75%, even at saturating doses of PDGF. PP2, an src kinase family inhibitor, inhibits Transwell migration in the presence of 7% serum with an IC_{50} of 80 ± 10 nM (inset). However, the inhibitory effect of 100 nM PP2 can be completely overcome with addition of sufficient PDGF (black squares). Data were normalized to the mean of cells migrating in the absence of PDGF and expressed as fold enhancement.

PDGF in this assay, addition of EGF overcomes this inhibition. By contrast, directly inhibiting myosin II with blebbistatin, an allosteric, small molecule inhibitor of this molecular motor (Limouze *et al.*, 2004), blocks Transwell migration, even in the presence of both PDGF and EGF. This is confirmed by the experimental results illustrated in Figure 1D. Incubation with EGF for 6 h induces Transwell migration with a hyperbolic dose–response relationship (Figure 1D, blue). In the presence of 30 µM blebbistatin, this migration is blocked more than 95%, even at saturating doses of EGF.

Gliomas frequently up-regulate multiple promigratory signaling pathways. We therefore examined the efficacy of blebbistatin in

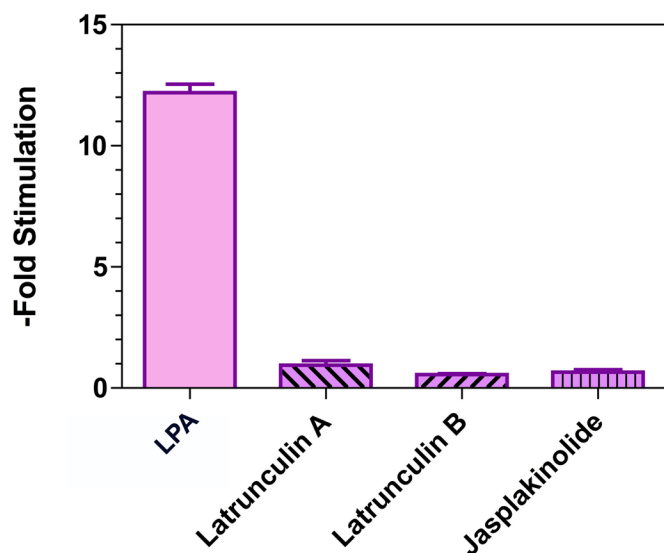


FIGURE 3: Effect of inhibitors of actin dynamics on migration of C6-EGFR cells through 3-µm Transwells. Data were normalized to the mean of cells migrating in the presence of latrunculin A and expressed as fold enhancement. Compared with stimulation with 1 µM LPA, 5 µM latrunculin A, 3 µM latrunculin B, and 200 nM jasplakinolide significantly block Transwell migration.

blocking Transwell migration of C6-EGFR cells in response to a range of concentrations of two additional ligands whose signaling pathways are frequently activated in gliomas—lysophosphatidic acid (LPA) and PDGF. The former stimulates glioma invasion through its activation of cell surface G protein-coupled receptors that in turn activate Rho and ROCK (Manning *et al.*, 1998), while the receptor for the latter is frequently expressed in human GBM (Wullich *et al.*, 1994; Nagane *et al.*, 1996; El-Obeid *et al.*, 1997; Maher *et al.*, 2001). We measured Transwell migration after 12 h of incubation with a range of concentrations of LPA (Figure 2A) and PDGF (Figure 2B), and this generated dose–response curves in both cases (Figure 2, blue). Blebbistatin effectively blocks both LPA- and PDGF-stimulated migration over a broad range of either ligand. Given these results, we would expect that blocking migration by targeting one or a few promigratory receptors should be readily overcome by simultaneously stimulating other promigratory receptors. This is consistent with our finding

that PP2, an inhibitor of both src family and EGFR tyrosine kinases (Kong *et al.*, 2010), blocks Transwell migration in the presence of 10% serum (Figure 2B, inset), but its effects can be completely overcome with sufficient PDGF (Figure 2B, black squares).

Although motility in a wide variety of systems requires dynamic polymerization of actin, a recent report that examined the effect of actin-depolymerizing agents (dihydrocytochalasin B and latrunculin A) on a human GBM cell line concluded that actin polymerization was not necessary for cell motility (Panopoulos *et al.*, 2011). However, this study examined glioma migration in a two-dimensional, barrier-free surface. As we have noted (Beadle *et al.*, 2008), studies of migration on these surfaces do not recapitulate the mechanical constraints that glioma cells experience while dispersing within the brain, and drugs that block glioma cell dispersion through brain do not alter motility when these cells are monitored on a coverslip. We have therefore examined the effect of inhibiting actin dynamics on the migration of C6 cells through 3-µm Transwell membranes; the results are depicted in Figure 3. As the figure shows, drugs that interfere with actin-polymerization dynamics, including latrunculin A, latrunculin B, and jasplakinolide, effectively block Transwell migration in response to serum ($p < 0.0001$). Our results, in conjunction with earlier findings (Beadle *et al.*, 2008; Panopoulos *et al.*, 2011), suggest glioma cells are highly flexible in how they move and have an established hierarchy of motility mechanisms shaped by the mechanical demands placed on them. Thus migrating on a barrier-free, two-dimensional surface, such as a coverslip, requires neither actin polymerization nor myosin II activity, so long as microtubule polymerization is present. By contrast, migrating through a more restrictive environment that requires glioma cells to extrude themselves through small pores requires both cytoskeletal components.

While our *in vitro* results support our hypothesis that direct inhibition of myosin II is more effective than indirect inhibition, brain tissue presents unique mechanical challenges and provides complex chemical cues to invading glioma cells that may not be entirely reproduced by the Transwell assay. We therefore next examined a more realistic model of tumor invasion, using two engineered rodent brain tumor models.

Condition	D ($\mu\text{m}^2/\text{h}$) mean \pm SE	n	Compared with	p value
Control	723 \pm 203	113	—	—
EGF	755 \pm 243	77	Control	0.977
EGF plus Iressa	32 \pm 8	59	Control EGF	<0.0001 <0.0001
EGF plus blebbistatin	34 \pm 7	105	Control EGF	<0.0001 <0.0001
EGF plus PDGF	874 \pm 191	104	Control EGF	0.27 0.34
EGF plus PDGF plus Iressa	660 \pm 70	106	EGF plus PDGF	0.42
EGF plus PDGF plus blebbi- statin	58 \pm 22	73	EGF plus PDGF	<0.0001
			EGF plus PDGF plus Iressa	<0.0001

TABLE 1: Cell dispersal rates for EGFR-positive cells in a model of gliomatosis cerebri.

Brain slice invasion assay using EGFR-expressing rat glial progenitor cells

We have shown that intracerebral injection of rat pups with a retrovirus encoding an EGFR-GFP fusion protein leads to the formation

of a diffusely infiltrative lesion consisting of infected glial progenitor cells that continue to proliferate and are unable to differentiate during the life span of the injected animal (Ivkovic *et al.*, 2008). The EGFR-positive cells are highly motile and express high levels of PDGFR α . We have also demonstrated that EGFR-GFP is phosphorylated in situ in the presence of EGF. We chose to first investigate this model system, as it is highly invasive and overexpresses a promigratory growth factor receptor. Furthermore, the resulting lesions histologically resemble gliomatosis cerebri, a form of glioma characterized by extensive infiltration of the brain

We injected retroviruses encoding EGFR-mCherry into the subcortical white matter of neonatal pups in order to examine the motility of transfected cells in the presence of various combinations of EGF, PDGF, Iressa, and blebbistatin (Table 1). After 5 d, we generated 300- μm -thick brain slices in the vicinity of the injection site, monitored the migration of EGFR-expressing cells over 10 h, and tracked the migratory paths of individual cells (Figure 4). Representative time-lapse videos resulting from these experiments are included as Supplemental Videos S1–S7. We transposed these paths to a common origin in order to generate the static Wind Rose plots depicted in Figure 4A. Visual inspection of these plots leads to several conclusions. First, while EGFR-expressing cells are motile under control conditions, adding exogenous EGF to 0.1 ng/ml does not appear to enhance motility further, implying that multiple other ligands are already present at high enough concentrations to stimulate invasion of EGFR-expressing cells. Second, unlike the results of our *in vitro* invasion assay with C6-EGFR(+) cells (Figure 1B), adding PDGF does not appreciably enhance tumor motility. Third, while Iressa effectively blocks EGF-stimulated motility, this inhibition can be overcome by adding PDGF. Finally, blebbistatin remains effective

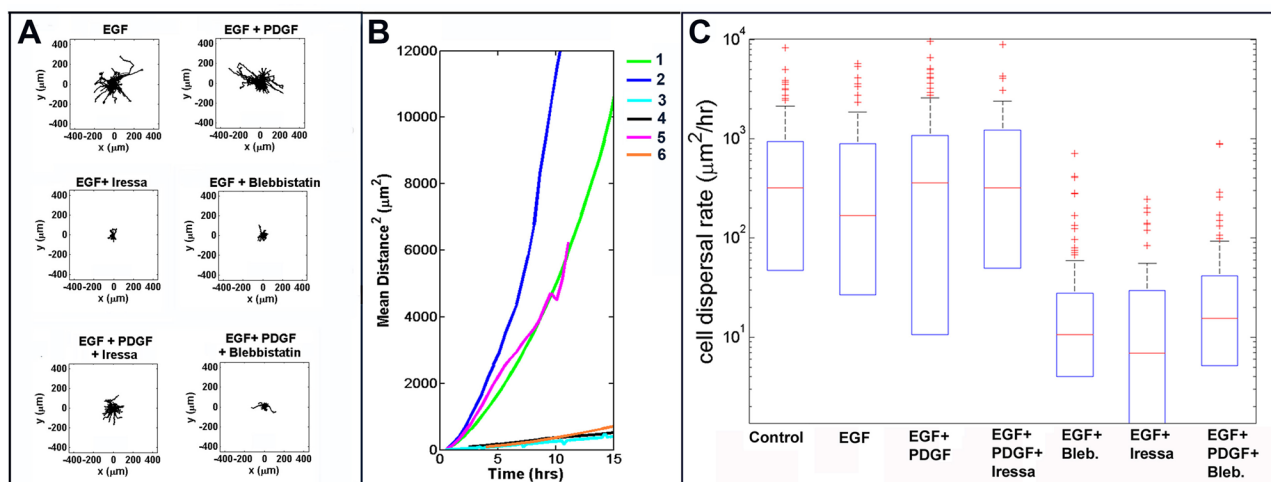


FIGURE 4: Migration of EGFR-mCherry expressing cells in a model of gliomatosis cerebri. (A) Migration of EGFR-mCherry-expressing cells was monitored in 300- μm -thick brain slices by time-lapse microscopy for 10 h. Individual cell tracks were transposed to a common origin to generate the resulting wind rose plots displayed in (A). Slices were treated with 0.1 ng/ml of EGF; EGF plus 100 ng/ml PDGF; EGF plus 10 μM Iressa; EGF plus 20 μM blebbistatin; EGF plus PDGF plus 10 μM Iressa; or EGF plus PDGF plus 20 μM blebbistatin. (B) MSD vs. time for the various treatments. The curves show the MSD the cells have traveled away from the common origin shown in the wind rose plots over time. The slope of the linear portion of the curves provides an estimate of the diffusion rate of the cells. Values of the diffusion constant (D) for each condition are summarized in Table 1. Code: EGF = 1; EGF + PDGF = 2; EGF + Iressa = 3; EGF + blebbistatin = 4; EGF + PDGF + Iressa = 5; EGF + PDGF + blebbistatin = 6. (C) Distribution of cell dispersal rates. The box plots show the distributions of dispersal rates of individual cells within a population. The middle red line shows the median dispersal rate; the top and bottom edges of the box are the 75th and 25th percentiles, respectively; the whiskers (black dashed lines) show the most extreme values not considered outliers; and the red +s are outliers. Notice that the vertical axis is log scale, so zero and negative values cannot be shown, and thus there are no bottom whiskers or outliers.

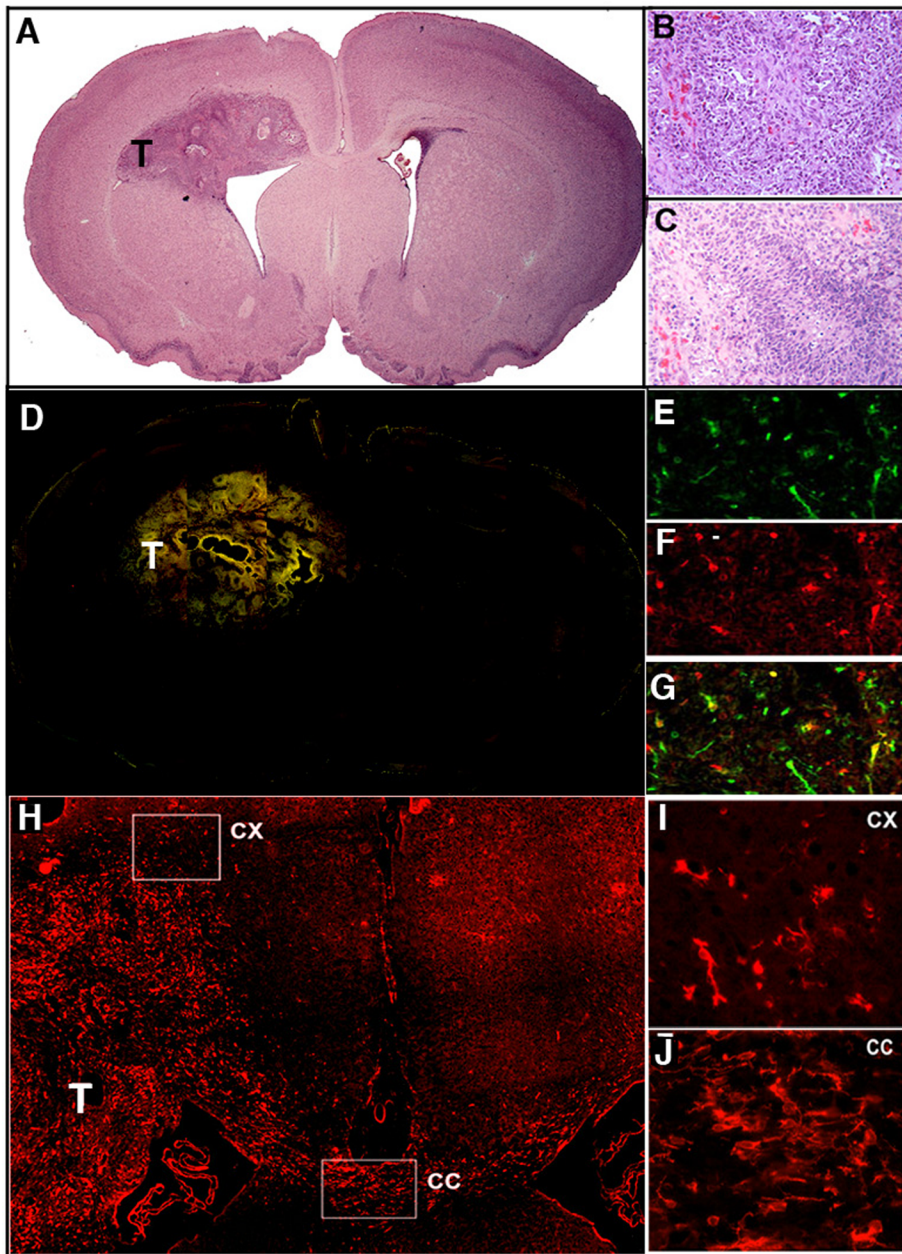


FIGURE 5: Coinjection of EGFR-mCherry- and PDGF-IRES-GFP-encoding retroviruses into the 3-d-old rat white matter induces the formation of GBM. (A) At 10-d postinjection, a tumor mass (T) is apparent (hematoxylin and eosin staining; 4× objective). With a 20× objective, the tumor is seen to demonstrate the hallmarks of GBM, including vascular proliferation (B) and pseudopalisading necrosis (C). (D) Montage of fluorescence micrographs (4× objective) of red and green cells show that the tumor mass is composed of both green PDGF-IRES-GFP-expressing cells (20× objective in E), red EGFR-mCherry-expressing cells (20× objective in F) and yellow double-infected cells (20× objective in G). (H) Low-power (4× objective) micrograph of mCherry fluorescence demonstrates EGFR(+) cells not only within the tumor mass (T), but also invading the cortex (CX) and corpus callosum (CC). This is also illustrated with a 10× objective for the cortex (I) and corpus callosum (J).

not only in the presence of EGF but also in the presence of EGF and PDGF combined.

To provide a more quantitative and statistically valid measure of the effects of ligands and inhibitors on migration, we also calculated the mean square displacement (MSD) of these cells as a function of time for each of the conditions depicted in Figure 4A. According to the persistent random walk model, the slope of a plot

of MSD versus time defines a diffusion constant (Table 1), which provides a quantitative measure of cell dispersion under each condition (Kim *et al.*, 2008). Figure 4B depicts plots of MSD versus time for various treatment conditions, and Figure 4C illustrates box plots demonstrating distributions of dispersal rates of individual cells within a population. Our *in vitro* studies with C6 cells suggest that blocking glioma migration by directly targeting myosin II remains effective in the presence of several simultaneously active signaling pathways. This conclusion is consistent with the values of dispersal rates listed in Table 1, derived from a more physiologically relevant assay of dispersion through brain tissue. However, we also note that unlike the simple *in vitro* invasion assays with C6 cells (Figures 1 and 2), in which the number of promigratory ligands can be accounted for and controlled, the corresponding situation in our brain tissue invasion assay is more complex, with our evidence suggesting that multiple promigratory pathways are likely activated. This suggests that studies of tumor invasion based solely on *in vitro* assays need to be correlated with corresponding assays involving physiologically relevant host tissue.

Our model of gliomatosis cerebri does not recapitulate the features of the more complex GBM. We therefore examined a more complex and clinically relevant model—a rodent GBM in which tumor cells secrete PDGF and express both PDGFR α and EGFR.

Brain slice invasion assay in a PDGF-secreting and EGFR- and PDGFR α -expressing rat GBM

We simultaneously injected rat pups intracerebrally with two Moloney-based retroviruses. The first, encoding for PDGF-B-hemagglutinin and GFP (PDGF-IRES-GFP), drives formation of a diffusely infiltrative tumor (Assanah *et al.*, 2006) that has all of the histological features of GBM (Figure 5). We have previously used this model to monitor the migration of retrovirus-infected tumor cells in culture slices generated from these tumors (Beadle *et al.*, 2008; Assanah *et al.*, 2009). The second encodes for the EGFR-mCherry fusion protein utilized in our model of gliomatosis cerebri (as discussed in the preceding section). Both the EGFR-expressing cells and the PDGF-secreting cells are motile, and could be seen to have dispersed long distances from the site of retroviral injection, with both red and green fluorescent cells found in the corpus callosum and the contralateral hemisphere (Figure 5). In this more complex system, the EGFR-mCherry-expressing cells, which also express endogenous PDGFR α , are stimulated by the

is cerebri (as discussed in the preceding section). Both the EGFR-expressing cells and the PDGF-secreting cells are motile, and could be seen to have dispersed long distances from the site of retroviral injection, with both red and green fluorescent cells found in the corpus callosum and the contralateral hemisphere (Figure 5). In this more complex system, the EGFR-mCherry-expressing cells, which also express endogenous PDGFR α , are stimulated by the

Condition	D ($\mu\text{m}^2/\text{hr}$) Mean \pm SE	n	Compared with	p value
Control	572 \pm 120	110	—	—
EGF	575 \pm 115	76	Control	0.965
EGF plus Iressa	395 \pm 224	73	Control EGF	0.217 0.239
EGF plus blebbistatin	50 \pm 7	134	Control EGF EGF plus Iressa	<0.0001 <0.0001 0.007

TABLE 2: Cell dispersal rates for EGFR-positive cells in model of GBM.

PDGF-expressing cells, which constitutively express and secrete PDGF. We performed time-lapse analysis and cell tracking of the EGFR-mCherry-expressing cells in the absence (Table 2, Control) and presence of 0.1 ng/ml EGF and various inhibitors (Table 2). Figure 6, A–C, depicts wind rose plots, MSD versus time plots, and box plots of dispersal rates, respectively, for the various conditions. Representative time-lapse videos resulting from these experiments are included as Supplemental Videos S8–S11. As in the case of the simpler gliomatosis model, we found that addition of EGF does not further enhance the rate of tumor cell dispersion (Table 2; $p = 0.965$). Endogenous production of PDGF in this GBM model appears to have the same effect as that of adding exogenous PDGF to the gliomatosis model—it eliminates the efficacy of Iressa, but is unable to overcome the inhibition of dispersion by blebbistatin (Table 2). As we discussed in our prior study (Beadle et al., 2008), blebbistatin effectively paralyzes movement of the cell body, but does not prevent dynamic extension and retraction of the cytoplasmic processes these cells generate.

Myosin IIA heavy chain phosphorylation occurs in GBM and is modulated by EGF signaling

Recent evidence indicates that EGF induces rapid phosphorylation of the myosin IIA heavy chain on Ser-1943 in breast carcinoma (Dulyaninova et al., 2007). Since our previous studies demonstrated that myosin IIA heavy chain expression is up-regulated in human and rodent gliomas (Beadle et al., 2008), we wished to see whether we could detect phosphorylation on Ser-1943 in human and rodent gliomas as well. We compared the levels of phospho-Ser-1943 myosin IIA relative to the total myosin IIA heavy chain in four human GBM specimens and five human temporal lobe specimens that were resected for control of intractable epilepsy. As illustrated in Figure 7, A and B, we found that levels of myosin IIA phosphorylation were on average twofold higher in tumor specimens. To examine the dynamics of EGF-mediated myosin II heavy chain phosphorylation, we treated C6-EGFR(–) and C6-EGFR(+) cells with 16.5 ng/ml EGF and performed immunoblots of the cell lysates to probe for the relative content of phospho-Ser-1943 myosin IIA after defined periods of EGF exposure. Results are summarized in Figure 7C. We found that addition of EGF to EGFR(+) C6 cells (Figure 7C, blue) produces a time-dependent rise in phospho-Ser-1943 heavy chain that, when compared with EGFR(–) cells (Figure 7C, red), reaches statistical significance by 15 min.

DISCUSSION

GBM growth and invasion can be stimulated by multiple signal transduction pathways that are frequently dysregulated

GBMs frequently contain genetic abnormalities that amplify or constitutively activate growth- and invasion-enhancing signal transduction pathways (Grzimir and Hemmings, 2010). The high frequency of these genetic abnormalities has served as an impetus for examining a variety of growth factor receptor antagonists in clinical trials for patients with GBM. Responses to these drugs, however, have been

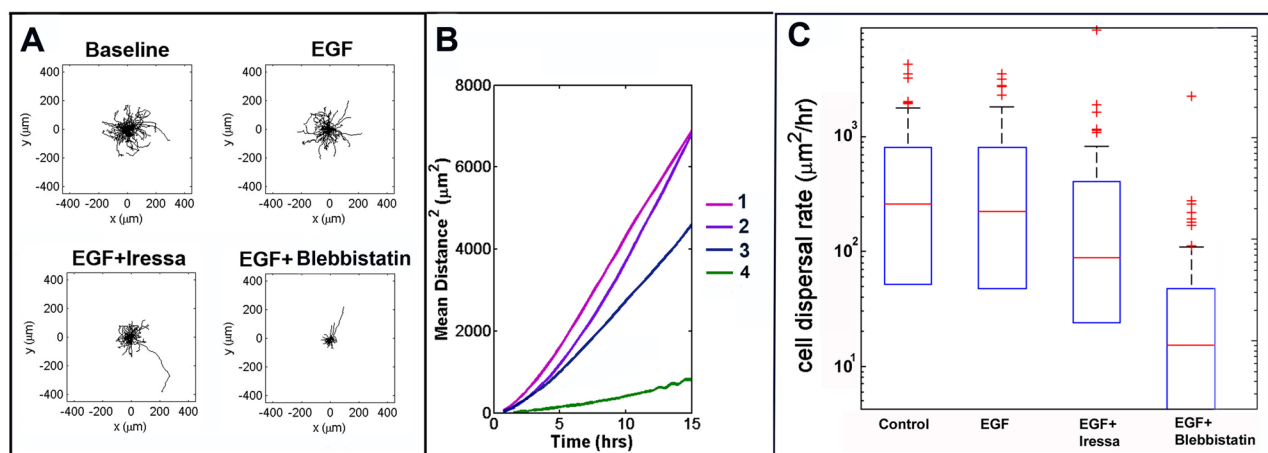


FIGURE 6: Migration of EGFR-mCherry-expressing cells in a model of GBM. (A) The panel depicts wind rose plots for EGFR(+) cell migration, as described in Figure 4. Slices were treated with medium alone (Baseline), 0.1 ng/ml of EGF, EGF plus 10 μM Iressa (EGF + Iressa), or EGF plus 20 μM blebbistatin (EGF + blebbistatin). (B) MSD vs. time, as described in Figure 4, for tumor cell populations and treatments. MSD curves show the MSD cells traveled away from their starting points (shown as a common origin in the wind rose plots (A)) over time. Values of the diffusion constant (D) are summarized in Table 2. Code: Baseline = 1; EGF = 2; EGF + Iressa = 3; EGF + blebbistatin = 4. (C) Distribution of cell dispersal rates among different treatments of tumor EGF cells. The box plots show the distributions of dispersal rates of individual cells within a population. The middle red line shows the median dispersal rate; the top and bottom edges of the box are the 75th and 25th percentiles, respectively; the whiskers (black dashed lines) show the most extreme values not considered outliers; and the red +s are outliers. Notice that the vertical axis is log scale, so zero and negative values cannot be shown, and thus there are no bottom whiskers or outliers.

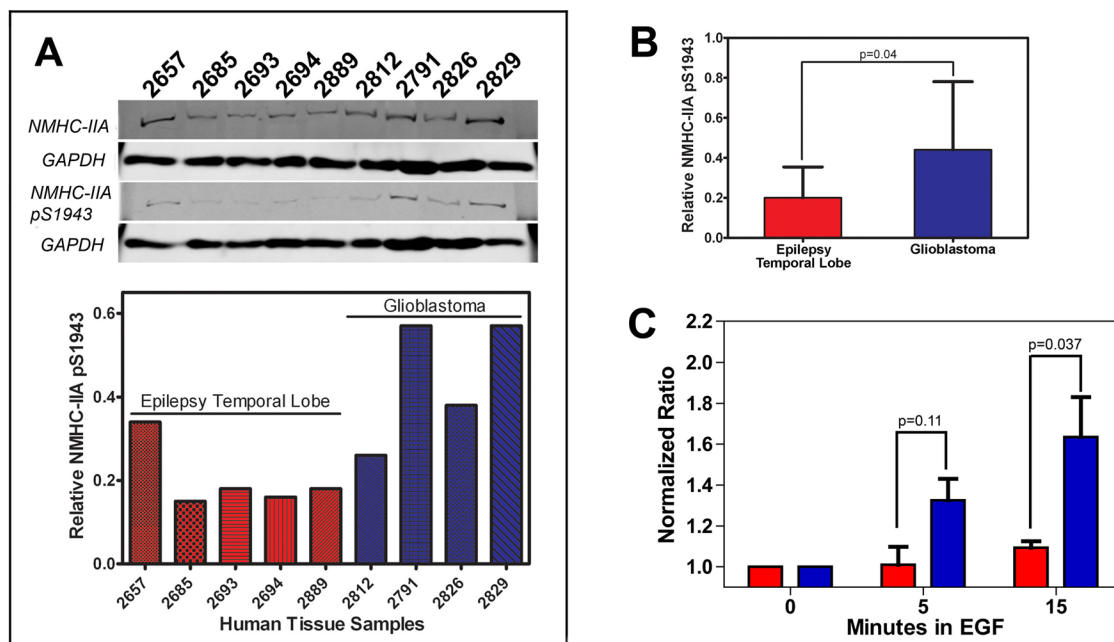


FIGURE 7: Myosin IIA heavy chain phosphorylation in GBM. (A) Immunoblot analysis of myosin IIA Ser-1943 phosphorylation in human tissue lysates derived from human epilepsy temporal lobe (red) or GBM (blue). GAPDH was used as a loading control. Relative phosphorylation levels were determined by dividing the myosin IIA pSer-1943/GAPDH ratio by the total myosin IIA/GAPDH ratio. (B) The normalized level of pSer-1943 myosin IIA is significantly increased in GBM samples (0.44 ± 0.15) vs. epileptic temporal lobes (0.20 ± 0.08). Values represent the mean \pm SD. (C) EGF-mediated increases in myosin IIA pSer-1943 in C6 (red) and C6-EGFR (blue) glioma cells as a function of time after EGF exposure. Cells were serum-starved and stimulated with 16.5 ng/ml EGF, and the phosphorylation status of the myosin IIA heavy chain was examined by immunoblot with an antibody that recognizes pSer-1943. Phosphorylation is expressed as the change relative to unstimulated cells. Values represent mean \pm SD for three (C6) and two (C6-EGFR) independent experiments.

limited in frequency and duration (de Groot and Gilbert, 2007; Rardon *et al.*, 2008). Although this may be due in part to problems in drug delivery, at least two other issues are likely contributors. The first of these is redundancy. GBMs frequently coexpress multiple growth factor receptors, including not only EGFR, but also PDGFR α and *c-met* (Wullich *et al.*, 1994; Nagane *et al.*, 1996; El-Obeid *et al.*, 1997; Maher *et al.*, 2001; Cancer Genome Atlas, 2008). The second issue is tumor heterogeneity. Anaplastic gliomas are heterogeneous tumors, and this is reflected in regional differences in the expression of mutant oncogenes and amplified receptors (Okada *et al.*, 2003; Ren *et al.*, 2007; Mott *et al.*, 2008; Parsons *et al.*, 2008). Thus some portions of these tumors may be insensitive to a specific cell-signaling inhibitor. These considerations imply there is a need to identify other targets of the invasion apparatus that are points at which these signal transduction pathways converge and are therefore likely to be less redundant. Our experiments in this study support our hypothesis that myosin II-dependent glioma invasion represents such a target.

Myosin II represents a point at which promigratory signal transduction pathways converge

In our prior study, we had shown that invasive glioma cells used myosin II to generate the contractile forces needed to squeeze their cell bodies through the small intercellular spaces that characterize brain white matter and cortex (Beadle *et al.*, 2008). In addition, more recent work from Kumar and colleagues has highlighted the role of myosin II isoforms in tuning migratory behavior to the mechanics of the tumor microenvironment (Sen *et al.*, 2009; Ulrich

et al., 2009). The two myosin II isoforms consistently expressed in gliomas (IIA and IIB) are both downstream effectors of multiple signal transduction pathways that are dysregulated in these tumors, including those stimulated by PDGF and EGF (Ben-Ya'acov and Ravid, 2003; Dulyaninova *et al.*, 2007). These signaling cascades converge on several kinases that modulate myosin II activity by phosphorylating its regulatory light chains and heavy chains (Manning *et al.*, 1998; Dulyaninova *et al.*, 2007). We had previously shown that stimulation of human GBM cells with promigratory ligands enhances regulatory light chain phosphorylation (Manning *et al.*, 1998); and in this study we find a similar enhancement of phosphorylation at Ser-1943, a site previously shown to be phosphorylated in response to EGF stimulation (Dulyaninova *et al.*, 2007). This leads us to make two predictions: 1) if promigratory signaling kinases, such as EGFR and PDGFR, overlap in their ability to stimulate glioma migration, then the effect of inhibiting one should be overcome by stimulating another; and 2) since myosin II is a point at which these signaling kinases converge, directly inhibiting myosin II with blebbistatin should remain effective in blocking glioma invasion, even if several upstream signaling receptors, such as EGFR or PDGFR α , are activated.

Our approach has been to investigate the relative efficacy of direct versus indirect inhibition of myosin II through a series of glioma invasion models of increasing complexity. Our results with the simplest invasion assay—EGFR-expressing C6 cells moving across 3- μ m Transwell membranes—support our predictions (Figures 1 and 2). First, both EGF and PDGF stimulate Transwell migration. Second, PDGF addition can reverse the anti-invasive effects that result from

blocking upstream elements in signaling cascades, including EGFR and *src* kinases, and vice versa. Third, direct inhibition of myosin II remains effective, even in the presence of saturating doses of PDGF, EGF, or LPA.

We used a series of experimental systems of increasing complexity, starting with a Transwell assay and following that with *ex vivo* tissue invasion assays of slice cultures generated from two brain tumor models—one that overexpresses EGFR and resembles gliomatosis cerebri, and a second model that overexpresses both EGFR and PDGF and resembles GBM. At a superficial level, our results using these brain invasion models are consistent with the Transwell results. Both suggest that while stimulation of a second signal transduction pathway with PDGF overcomes the effect of an EGFR inhibitor, it cannot overcome direct inhibition of myosin II with blebbistatin. Nevertheless, Transwell assays do not recapitulate every feature found in a bone fide glioma. In particular, the motile behavior of the EGF- and PDGF-stimulated tumor cells that we observed in our assay implies that there are likely to be multiple ligands in tumor-infiltrated brain that may be stimulating pathways downstream of EGFR and PDGFR α , as well as other receptors that are dysregulated in glioma. However, the reverse may also be true, as drugs such as blebbistatin can affect cellular responses to shear forces (LeDuc *et al.*, 2010), and they could conceivably affect the mechanics of brain tissue in such a way as to independently alter how glioma cells disperse. By contrast, this concern would not apply to assays that utilize Transwell membranes. Hence we conclude that both types of studies may be necessary to dissect mechanisms of cellular dispersion in glioma, as well as in other motile systems.

In a previous study, it was noted that treatment with Y27632 or transfection with a dominant-negative ROCK construct moderately enhanced migration of glioma cell lines on two-dimensional migration assays and through Transwell membranes (Salhia *et al.*, 2005). We note that the authors of that study did not specify the pore size of the Transwell membranes they used, and as we demonstrated in our prior study (Beadle *et al.*, 2008), this parameter is crucial in determining the need for myosin II in glioma migration. In particular, we found that while Y27632 and blebbistatin blocked migration of glioma cells through Transwell pores of 3- μ m diameter, they had no effect when pore size was increased to 8 μ m. We also found that Y27632 profoundly inhibits glioma cell migration through brain tissue sections, in which intercellular spaces are typically submicrometer in size (Thorne and Nicholson, 2006). Thus, as in the case of inhibitors of actin polymerization (Panopoulos *et al.*, 2011), we expect that the effect of inhibiting myosin II will vary with the type of assay used. This argues that results from experiments using two-dimensional or Transwell assays need to be corroborated by corresponding experiments using tissue invasion assays, as we have done in this study.

While we have shown in this study that targeting myosin II produces a robust inhibition of tumor dispersion within brain tissue, we do note that a few tumor cells escape the effects of blebbistatin (Figures 4 and 6). This may reflect the fact that GBM cells migrate within two discrete microenvironments. The first is composed of gray and white matter structures, including cortex, striatum, and white matter, whose extracellular spaces are delimited by cell processes and which contain sparse extracellular matrix. The second is the perivascular space, which contains abundant extracellular matrix, which forms a discrete layer sandwiched between the endothelial cells and the astrocyte endfeet (Giese and Westphal, 1996; Wolburg *et al.*, 2009). Whether these “blebbistatin-resistant” cells represent a subpopulation migrating within the perivascular compartment will need to be investigated in future studies.

Myosin II may be a valid target for new therapeutic strategies that block GBM invasion

While the pathways stimulated by EGF and PDGF are frequently up-regulated in GBM, other pathways are also frequently activated, including those downstream of *c-met* and *src* kinase family members (Angers-Loustau *et al.*, 2004; Lund *et al.*, 2006). This speaks to the importance of finding nonredundant mediators of the malignant phenotype of GBM whose inhibition will produce an effect regardless of how many upstream signaling pathways are activated. In this study, we have used experimental systems that allow us to systematically compare the relative efficacy of two approaches to blocking glioma invasion—targeting of upstream promigratory receptors that are frequently dysregulated in GBM versus direct targeting of myosin II. Our results lead us to propose that myosin II is a point at which many of these dysregulated pathways converge, it is not redundant, and its loss cannot be overcome by utilizing nonmyosin-dependent motility mechanisms that appear to be sufficient to drive cell motility in other experimental systems (De Lozanne and Spudich, 1987).

One potential limitation of any tumor-targeting strategy is toxicity. While we found that blocking actin dynamics also inhibited glioma migration both *in vitro* and in brain slices, we note that actin is universally expressed in cells, and its dynamic polymerization underlies many components of cell physiology, including intracellular transport. We would expect therefore that systemic or intracerebral administration of actin-polymerization inhibitors would have unacceptable toxicities. By contrast, the functions of myosin II are more delimited. Furthermore, myosin II isoforms (IIA, IIB, and IIC) are not equally expressed in all tissues. Thus we have shown that while the IIA isoform is minimally expressed in normal brain, it is markedly up-regulated in gliomas and neovasculature (Beadle *et al.*, 2008). This may provide a selective targeting strategy, since the calmodulin family member S100A4, which is up-regulated in metastatic carcinomas and GBMs (Camby *et al.*, 1999; Suemizu *et al.*, 2007), selectively regulates myosin IIA by allowing it to rapidly redistribute in migrating cells. Phenothiazines, which cross the blood–brain barrier, have been in clinical use for many years and can inhibit S100A4 by inducing protein oligomerization (Malashkevich *et al.*, 2010). Furthermore, an orally bioavailable ROCK inhibitor, fasudil, is currently in clinical use for the treatment of unstable angina and pulmonary hypertension, and it has been found to block metastasis of breast carcinoma in rodent models (Masumoto *et al.*, 2002; Shimokawa, 2002; Shimokawa *et al.*, 2002; Mohri *et al.*, 2003; Ying *et al.*, 2006). Thus drugs that inhibit myosin II function are already in clinical use, and ongoing studies are underway in our laboratories to examine the durability of these and other inhibitory strategies in the treatment of GBM.

MATERIALS AND METHODS

Retrovirus production

An EGFR-GFP plasmid was generated as previously described (Sun *et al.*, 2005) from the original pCLE retroviral vector (Gaiano *et al.*, 1999) and were a kind gift from Sally Temple (SUNY, Albany). An EGFR-mCherry plasmid was generated by replacing GFP with an mCherry reporter gene (pmCherry-N1; Clontech, Mountain View, CA) and was a kind gift from Tim Gershon (University of North Carolina, Chapel Hill). pQ PDGF-hemagglutinin-IRES-eGFP (PDGF-IRES-GFP) was generated as previously described (Assanah *et al.*, 2006). Replication-deficient viruses with vesicular stomatitis virus (vsv)-G coats were generated from these constructs, as described previously (Kakita and Goldman, 1999). Viral titers were determined in colony-forming units by incubating C6 glioma cells with serial dilutions of retrovirus in 10-fold steps. At 48-h postinfection, the

GFP-positive cell clusters were counted, and the titer of all generated viruses was 10^5 – 10^6 viral particles/ μ l.

Retroviral injections

We anesthetized neonatal Sprague Dawley rats (P3) by submerging them in ice water for 8 min. The heads were then placed in a stereotaxic apparatus (Stoelting, Avondale, IL) and virus was injected into the rostral subcortical white matter at stereotaxic coordinates 2-mm lateral and 1-mm rostral to the bregma. A 33-gauge Hamilton microsyringe (Reno, NV) was inserted to a depth of 1.5 mm, and 1–2 μ l of virus was injected at a rate of 0.2 μ l/min. All animal experiments were performed according to the guidelines of the Institutional Animal Care and Use Committee at Columbia University.

Staining procedures

Animals were anesthetized with ketamine–xylazine at 10 d postinjection (10 dpi), and underwent cardiac perfusion with 15 ml of phosphate-buffered saline (PBS) and 15 ml of 4% paraformaldehyde. Brains were fixed for 24 h and transferred to PBS until used. Fixed brains were cryopreserved in 30% sucrose in 1X PBS and cryosectioned at 12 μ m, and sections were stored at 80°C until used. Antibodies used included: sheep anti-EGFR (1:100; Millipore, Billerica, MA), mouse anti-phospho-EGFR-Y1068 (1:50; Cell Signaling Technology, Beverly, MA), rabbit anti-phospho-EGFR-Y1173 (1:100; Stressgen, San Diego, CA), and goat anti-PDGFR (1:80; R & D Systems, Minneapolis, MN). Sections were blocked with 10% horse serum, 0.1% Triton X-100 in 1X PBS for 30 min before an overnight incubation with primary antibody at 4°C. On the following day, the sections were washed extensively and incubated in secondary antibody for 1 h at room temperature. FITC- and TRITC-conjugated secondary antibodies were used for double fluorescence (FITC: Jackson ImmunoResearch, West Grove, PA; TRITC: Alexa Fluor, Invitrogen, Carlsbad, CA). Sections were washed extensively again and stained with Hoechst 33342 (Invitrogen) for nuclear visualization.

Transwell migration assay

Fluoroblok transfilters (BD Biosciences, San Jose, CA) were coated with either 10% rat tail collagen, type I (BD Biosciences) or 3 μ g/ml purified human vitronectin (Invitrogen) in sterile, deionized water at 37°C for 1 h. Transfilter migration was assayed after 6 or 12 h of incubation at 37°C, as previously described (Beadle *et al.*, 2008). A two-tailed *t* test for the mean was used to assess the difference between the mean values of migration across experimental conditions.

Cell lines and cell culture

C6 glioma cells were used to generate two new cell lines—C6-EGFR-GFP and C6-EGFR-mCherry—via retroviral infection. Infected cells were fluorescence activated cell-sorted and cultured in 1:1 DMEM:F-12 nutrient mixture (Ham's) supplemented with GlutaMAX and 10% heat-inactivated fetal bovine serum (Invitrogen). Cells were maintained at 37°C with 5% CO₂.

Time-lapse microscopy of cell migration in brain slice

Rat pups injected with EGFR-GFP, EGFR-mCherry, or a combination of PDGF-IRES-GFP and EGFR-mCherry were killed by decapitation. Singly injected animals were killed at 5–7 dpi and coinjected animals at 10–12 dpi. Brains were isolated, and 300- μ m coronal sections of the injected hemispheres were made using a McIlwain Tissue Chopper (Campden Instruments, Loughborough, United Kingdom). The sections were transferred onto a 0.4- μ m culture plate insert (Millipore) and placed in a 6-well glass bottom plate with (MatTek, Ashland, MA), with 1000 μ l of serum-free medium per well. The

time-lapse experiments were performed in a stage-mounted incubator with CO₂ and temperature control, using a Nikon TE2000 inverted fluorescence microscope (Melville, NY), as previously described (Beadle *et al.*, 2008). Images were acquired at 40 \times magnification at 3-min intervals for up to 24 h. Results from a minimum of three separate experiments were pooled for data analysis.

Quantitative analysis of glioma cell migration

Individual cell tracks from time-lapse microscopy were plotted to a common origin to generate wind rose plots for spatial comparison of the effective spread of the cells across experimental conditions. By considering all combinations of elapsed times possible for each of the cells, we computed the MSD for the tracked cells within each experimental condition. The slope of the linear portion of the MSD curve was used to generate a diffusion/dispersal rate constant for each of the cells (Stokes *et al.*, 1991). This diffusion coefficient reflects the rate of spread of a population of cells with this dispersal pattern. A two-tailed *t* test for the mean was used to assess the difference between the mean cellular diffusion rates across experimental conditions.

Immunoblot analysis

Protein samples (cell lines and human tissue) were separated on parallel 8% SDS-PAGE, which was followed by immunoblotting with a glyceraldehyde-3-phosphate dehydrogenase (GAPDH) monoclonal antibody (#G8795; Sigma-Aldrich, St. Louis, MO) and either the pSer-1943 myosin IIA polyclonal antibody (rat cells: #5026; Cell Signaling Technology; human tissue: #AB2974; Millipore) or an antibody that recognizes total myosin IIA (rat cells: #WH0004627M3; Sigma; human tissue: Dulyaninova *et al.*, 2007). Immunoreactive proteins were detected using LI-COR Odyssey version 3.0 (LI-COR Biosciences, Lincoln, NE). Total myosin IIA and pSer-1943 myosin IIA were normalized to GAPDH to control for differences in loading. Relative phosphorylation was determined by dividing the pSer-1943 myosin IIA/GAPDH ratio by the total myosin IIA/GAPDH ratio. Relative phosphorylation was expressed as the change relative to unstimulated cells.

Human tissue specimens

Fresh human GBM and temporal lobe specimens were obtained according to Columbia University Institutional Review Board Guidelines (IRB protocol AAAAA4666). Tissue samples were obtained and immediately frozen in liquid nitrogen. Samples were stored at –80°C until used for immunoblot analysis.

ACKNOWLEDGMENTS

This work has been supported by a grant from Voices Against Brain Cancer and from the National Institutes of Health (R56-NS066992 to S.S.R. and P.C. and P01-CA100324 to A.R.B.).

REFERENCES

- Angers-Loustau A, Hering R, Werbowetski TE, Kaplan DR, Del Maestro RF (2004). Src regulates actin dynamics and invasion of malignant glial cells in three dimensions. *Mol Cancer Res* 2, 595–605.
- Assanah M, Lochhead R, Ogden A, Bruce J, Goldman J, Canoll P (2006). Glial progenitors in adult white matter are driven to form malignant gliomas by platelet-derived growth factor-expressing retroviruses. *J Neurosci* 26, 6781–6790.
- Assanah MC, Suzuki SO, Chen A, Bruce JN, Goldman JE, Canoll P (2009). PDGF stimulates the massive expansion of glial progenitors in the neonatal forebrain. *Glia* 57, 1835–1847.
- Beadle C, Assanah MC, Monzo P, Vallee R, Rosenfeld SS, Canoll P (2008). The role of myosin II in glioma invasion of the brain. *Mol Biol Cell* 19, 3357–3368.
- Ben-Ya'acov A, Ravid S (2003). Epidermal growth factor-mediated transient phosphorylation and membrane localization of myosin II-B are required for efficient chemotaxis. *J Biol Chem* 278, 40032–40040.

- Buckner JC, O'Fallon JR, Dinapoli RP, Schomberg PJ, Farr G, Schaefer P, Giannini C, Scheithauer BW, Ballman KV (2007). Prognosis in patients with anaplastic oligastrocytoma is associated with histologic grade. *J Neurooncol* 84, 279–286.
- Burger PC, Dubois PJ, Schold SC, Jr, Smith KR, Jr, Odom GL, Crafts DC, Giangaspero F (1983). Computerized tomographic and pathologic studies of the untreated, quiescent, and recurrent glioblastoma multiforme. *J Neurosurg* 58, 159–169.
- Burger PC, Kleihues P (1989). Cytologic composition of the untreated glioblastoma with implications for evaluation of needle biopsies. *Cancer* 63, 2014–2023.
- Cancer Genome Atlas Research Network (2008). Comprehensive genomic characterization defines human glioblastoma genes and core pathways. *Nature* 455, 1061–1068.
- Cancer Genome Atlas Research Network (2010). Comprehensive genomic characterization defines human glioblastoma genes and core pathways. *Nature* 455, 1061–1068.
- Camby I et al. (1999). Supranuclear pyclostoma astrocytomas, astrocytomas, anaplastic astrocytoma and glioblastoma are characterized by a differential expression of S100 proteins. *Brain Pathol* 9, 1–19.
- de Groot JF, Gilbert MR (2007). New molecular targets in malignant gliomas. *Curr Opin Neurol* 20, 712–718.
- De Lozanne A, Spudich JA (1987). Disruption of the *Dictyostelium* myosin heavy chain gene by homologous recombination. *Science* 236, 1086–1091.
- Dulyaninova NG, House RP, Betapudi V, Bresnick AR (2007). Myosin-IIA heavy-chain phosphorylation regulates the motility of MDA-MB-231 carcinoma cells. *Mol Biol Cell* 18, 3144–3155.
- El-Obeid A, Bongcam-Rudoff E, Sorby M, Ostman A, Niser M, Westermark B (1997). Cell scattering and migration induced by autocrine transforming growth factor alpha in human glioma cells in situ. *Cancer Res* 57, 5598–5604.
- Gaiiano N, Kohtz JD, Turnbull DH, Fishell G (1999). A method for rapid gain-of-function studies in the mouse embryonic nervous system. *Nat Neurosci* 9, 812–819.
- Giese A, Westphal M (1996). Glioma invasion in the central nervous system. *Neurosurgery* 39, 235–250; discussion 250–252.
- Grzimir M, Hemmings BA (2010). Deregulated signaling networks in human brain tumours. *Biochim Biophys Acta* 1804, 476–483.
- Hoelzinger DB, Demuth T, Berens ME (2007). Autocrine factors that sustain glioma invasion and paracrine biology in the brain microenvironment. *J Natl Cancer Inst* 99, 1583–1593.
- Ivkovic S, Canoll P, Goldman JE (2008). Constitutive EGFR signaling in oligodendrocyte progenitors leads to diffuse hyperplasia in postnatal white matter. *J Neurosci* 28, 914–922.
- Kakita A, Goldman JE (1999). Patterns and dynamics of SVZ cell migration in the postnatal forebrain: monitoring living progenitors in slice preparations. *Neuron* 23, 461–472.
- Kim HD, Guo TW, Wu AP, Wells A, Gertler FB, Lauffenburger DA (2008). Epidermal growth factor-induced enhancement of glioblastoma cell migration in 3D arises from an intrinsic increase in speed but an extrinsic matrix- and proteolysis-dependent increase in persistence. *Mol Biol Cell* 19, 4249–4259.
- Kong L, Deng Z, Shen H, Zhang Y (2010). Src family kinase inhibitor PP2 efficiently inhibits cervical cancer cell proliferation through down-regulating phospho-Src-Y416 and phospho-EGFR-Y1173. *Mol Cell Biochem* 348, 11–19.
- LeDuc Q, Shi Q, Blonk I, Sonnenberg A, Wang N, Leckbanbd D, deRoosij J (2010). Vinculin potentiates E-cadherin mechanosensing and is recruited to actin-anchored sites within adherens junctions in a myosin II-dependent manner. *J Cell Biol* 189, 1107–1115.
- Lim DA, Cha S, Mayo MC, Chen MH, Keles E, VandenBerg S, Berger MS (2007). Relationship of glioblastoma multiforme to neural stem cell regions predicts invasive and multifocal tumor phenotype. *Neuro Oncol* 9, 424–429.
- Limouze J, Straight AF, Mitchison T, Sellers JR (2004). Specificity of blebbistatin, an inhibitor of myosin II. *J Muscle Res Cell Motil* 25, 337–341.
- Lund CV, Nguyen MT, Owens GC, Pakchoian AJ, Shaterian A, Kruse CA, Eliceiri BP (2006). Reduced glioma infiltration in Src-deficient mice. *J Neurooncol* 78, 19–29.
- Maher EA, Furnari FB, Bachoo RM, Rowitch DH, Louis DN, Cavenee WK, DePinho RA (2001). Malignant glioma: genetics and biology of a grave matter. *Genes Dev* 15, 1311–1333.
- Malashkevich VN, Dulyaninova NG, Ramagopal UA, Liriano MA, Varney KM, Knight D, Brenowitz M, Weber DJ, Almo SC, Bresnick AR (2010). Phenothiazines inhibit S100A4 function by inducing protein oligomerization. *Proc Natl Acad Sci USA* 107, 8605–8610.
- Manning TJ, Jr, Rosenfeld SS, Sontheimer H (1998). Lysophosphatidic acid stimulates actomyosin contraction in astrocytes. *J Neurosci Res* 53, 343–352.
- Masumoto A, Mohri M, Shimokawa H, Urakami L, Usui M, Takeshita A (2002). Suppression of coronary artery spasm by the Rho-kinase inhibitor fasudil in patients with vasospastic angina. *Circulation* 105, 1545–1547.
- Mohri M, Shimokawa H, Hirakawa Y, Masumoto A, Takeshita A (2003). Rho-kinase inhibition with intracoronary fasudil prevents myocardial ischemia in patients with coronary microvascular spasm. *J Am Coll Cardiol* 41, 15–19.
- Mott RT, Turner KC, Bigner DD, McLendon RE (2008). Utility of EGFR and PTEN numerical aberrations in the evaluation of diffusely infiltrating astrocytoma. Laboratory investigation. *J Neurosurg* 108, 330–335.
- Nagane M, Coufai F, Lin H, Bogler O, Cavenee WK, Huang HJ (1996). A common mutant epidermal growth factor receptor confers enhanced tumorigenicity on human glioblastoma cells by increasing proliferation and reducing apoptosis. *Cancer Res* 27, 25639–25645.
- Norden AD, et al. (2008). Bevacizumab for recurrent malignant gliomas: efficacy, toxicity, and patterns of recurrence. *Neurology* 70, 779–787.
- Okada Y, Hurwitz EE, Esposito JM, Brower MA, Nutt CL, Louis DN (2003). Selection pressure of TP53 mutation and microenvironmental location influence epidermal growth factor receptor gene amplification in human glioblastomas. *Cancer Res* 63, 413–416.
- Panopoulos A, Howell M, Fotadar R, Margolis RL (2011). Glioblastoma motility occurs in the absence of actin polymer. *Mol Biol Cell* 22, 2212–2220.
- Parsons DW et al. (2008). Core signaling pathways in human pancreatic cancers revealed by global genomic analyses. *Science* 321, 1807–1812.
- Reardon DA et al. (2008). Randomized phase II study of cilengitide, and integrin-targeting arginine-glycine-aspartic acid peptide, in recurrent glioblastoma multiforme. *J Clin Oncol* 26, 5610–5617.
- Ren ZP, Olofsson T, Qu M, Hesselager G, Soussi T, Kalimo H, Smits A, Nister M (2007). Molecular genetic analysis of p53 intratumoral heterogeneity in human astrocytic brain tumors. *J Neuropathol Exp Neurol* 66, 944–954.
- Salhia B, Frederieke Rutten F, Mitsutoshi Nakada M, Beaudry C, Berens M, Allison Kwan A, Rutka JT (2005). Inhibition of rho-kinase affects astrocytoma morphology, motility, and invasion through activation of rac1. *Cancer Res* 65, 8792–8800.
- Scherer H (1940). Cerebral astrocytomas and their derivatives. *Am J Cancer* 1, 159–198.
- Sen S, Dong M, Kumar S (2009). Isoform specific contributions of α actinin to glioma cell mechanobiology. *PLoS One* 4, e8427.
- Shimokawa H (2002). Rho-kinase as a novel therapeutic target in treatment of cardiovascular diseases. *J Cardiovasc Pharmacol* 39, 319–327.
- Shimokawa H, et al. (2002). Anti-anginal effects of fasudil, a Rho-kinase inhibitor, in patients with stable effort angina: a multicenter study. *J Cardiovasc Pharmacol* 40, 751–761.
- Stokes CL, Lauffenburger DA, Williams SK (1991). Migration of individual microvessel endothelial cells: stochastic model and parameter measurement. *J Cell Sci* 99, 419–430.
- Stommel JM, et al. (2007). Coactivation of receptor tyrosine kinases affects the response of tumor cells to targeted therapies. *Science* 318, 287–290.
- Strawn LM, Mann E, Elliger SS, Chu ML, Germain LL, Niederfellner G, Ulrich A, Shawver LK (1994). Inhibition of glioma cell growth by a truncated platelet-derived growth factor- β receptor. *J Biol Chem* 269, 21215–21222.
- Stupp R, Hegi ME, Gilbert MR, Chakravarti A (2007). Chemoradiotherapy in malignant glioma: standard of care and future directions. *J Clin Oncol* 25, 4127–4136.
- Suemizu H, Monnai M, Ohnishi Y, Ito M, Tamaoki N, Nakamura M (2007). Identification of a key molecular regulator of liver metastasis in human pancreatic carcinoma using a novel quantitative model of metastasis in NOD/SCID/ycnull (NOG) mice. *Int J Oncol* 31, 741–751.
- Sun Y, Goderie SK, Temple S (2005). Asymmetric distribution of EGFR receptor during mitosis generates diverse CNS progenitor cells. *Neuron* 45, 873–886.
- Svitkina TM, Verkhovskiy AB, McQuade KM, Borisy GG (1997). Analysis of actin-myosin II system in fish epidermal keratocytes: mechanism of cell body translocation. *J Cell Biol* 139, 397–415.
- Thorne RG, Nicholson C (2006). In vivo diffusion analysis with quantum dots and dextrans predicts the width of brain extracellular space. *Proc Natl Acad Sci USA* 103, 5567–5572.
- Ulrich TA, de Juan Pardo EM, Kumar S (2009). The mechanical rigidity of the extracellular matrix regulates the structure, motility, and proliferation of glioma cells. *Cancer Res* 69, 4167–4174.
- Ying H, Biroc SL, Li WW, Alicke B, Xuan JA, Pagla R, Ohashi Y, Okada T, Kamata Y, Dinter H (2006). The Rho kinase inhibitor fasudil inhibits tumor progression in human and rat tumor models. *Mol Cancer Ther* 5, 2158–2164.
- Wolburg H, Noell S, Mack A, Wolburg-Buchholz K, Fallier-Becker P (2009). Brain endothelial cells and the gliovascular complex. *Cell Tissue Res* 335, 75–96.
- Wullich B, Sattler HP, Fischer U, Meese E (1994). Two independent amplification events on chromosome 7 in glioma: amplification of the epidermal growth factor receptor gene and amplification of the oncogene MET. *Anticancer Res* 14, 577–579.